Efficient Modeling of Impulsive ELF Antipodal Propagation About the Earth Sphere Using an Optimized Two-Dimensional Geodesic FDTD Grid

Jamesina J. Simpson, *Student Member, IEEE,* and Allen Taflove, *Fellow, IEEE*

Abstract—This letter reports the initial application of a geodesic finite-difference time-domain (FDTD) grid to model impulsive extremely low frequency electromagnetic wave propagation about the Earth sphere. The two-dimensional transverse-magnetic grid is comprised entirely of hexagonal cells, except for a small fixed number of pentagonal cells needed for grid completion. Grid-cell areas and locations are optimized to yield a smoothly varying area difference between adjacent cells, thereby maximizing numerical convergence. The new FDTD grid model is considerably superior to our previously reported latitude-longitude grid because it is simpler to construct, avoids geometrical singularities at the poles, executes about 14 times faster, provides much more isotropic wave propagation, and permits an easier interchange of data with state-of-the-art Earth-simulation codes used by the geophysics community. We verify our new model by conducting numerical studies of impulsive antipodal propagation and the Schumann resonance.

Index Terms—Antipodal propagation, extremely low-frequency (ELF), finite-difference time-domain (FDTD), geodesic grid, Schumann resonance, sphere.

I. INTRODUCTION

PROPAGATION of extremely low-frequency (ELF: 3 Hz–3 kHz) and very low-frequency (VLF: 3–30 kHz) electromagnetic waves in the Earth-ionosphere waveguide is a problem having a rich history of theoretical investigation extending over many years (see, for example, [1]–[6]). Currently, ELF/VLF propagation phenomena form the physics basis of important remote-sensing investigations of lightning and sprites [7], global temperature change [8], subsurface structures [9], and potential earthquake precursors [10].

Simpson and Taflove [11]–[15] and Hayakwa *et al.* [16], [17] reported the initial applications of the finite-difference time-domain (FDTD) [18] method to model the complete Earth-ionosphere waveguide at ELF. Both groups used spherical-coordinate, latitude-longitude grids based upon fundamental work by Holland [19]. Hayakwa *et al.* reported no improvements relative to Holland's grid, which is subject to increasing space-cell eccentricity upon approaching the poles due to converging lines of longitude. In contrast, Simpson and Taflove reported means to reduce the eccentricity of cells in the polar regions by a novel adaptive cell-combining technique applied to adjacent grid-cells in the east-west direction. This permits maintenance of the time-step at nearly the level allowed by the Courant stability condition for the square equatorial cells, yielding a greatly improved computational efficiency. Relative to data in the literature, the Simpson–Taflove technique was demonstrated to provide propagation modeling results accurate to within about ± 1 dB over the ELF range 50–500 Hz using only a laboratory computer to generate a high-resolution ($\sim 40 \times 40 \times 5$ km) three-dimensional (3-D) model of the global Earth-ionosphere cavity within ± 100 km of sea level [14].

While the latitude–longitude gridding technique of [11]–[13] has shown promise for whole-Earth models of ELF propagation, it still requires the use of a large parallel computer to model fine-grained details of the lithosphere that may be important for simulations of earthquake precursors and remote sensing of mineral deposits. Therefore, we have pursued alternative whole-Earth meshes that have the potential for improved efficiency. In this spirit, this letter reports a new geodesic FDTD grid model for the Earth-sphere that is considerably superior to our previously reported latitude-longitude grid. Namely, the geodesic FDTD grid is: 1) simpler to construct (avoiding the need for grid-cell combinations upon approaching the poles); 2) executes about 14-times faster; 3) provides much more isotropic wave propagation; and 4) permits an easier interchange of data with state-of-the-art Earth-simulation codes used by the geophysics community. Here, the grid is comprised entirely of hexagonal cells except for a small fixed number (12) of pentagonal cells needed for grid completion [20]. Grid-cell areas and locations are optimized to yield a smoothly varying area difference between adjacent cells, thereby maximizing numerical convergence [21].

II. GEODESIC FDTD GRID

Fig. 1 illustrates an example of the layout of a spherical geodesic grid for the two-dimensional (2-D) transverse-magnetic (TM) case of Maxwell's equations. This sample grid has a total of 642 planar cells, of which 630 are hexagons and 12 are pentagons [20]. For purposes of efficient mapping into the computer memory, this grid can be divided into five equal panels of size $im5 \times jm$ cells, where $im5 = 18$ and $jm = 10$. Fig. 2(a) shows the five grid panels of Fig. 1 after unwrapping and stretching them flat. The cells at the North and South Poles can be arbitrarily connected to any of the five panels. Fig. 2(b) illustrates how the five grid panels of Fig. 1 can be assigned
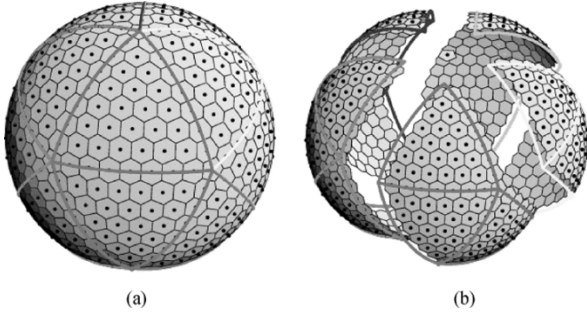
Fig. 1.   General layout of a 642-cell, 2-D geodesic grid covering the complete Earth-sphere. Each grid cell is planar. The grid is divided into five equal panels with $im5 = 18$ and $jm = 10$ [20].

logically Cartesian coordinates, and how all five panels can then be laid side-by-side to constitute an overall ($im = 90$ and $jm = 10$) logically Cartesian grid. This powerful interpretation of a spherical geodesic grid as a single logically Cartesian grid for purposes of efficient computer processing can be implemented for a variety of meshing densities over the sphere, as shown in Table I.

Regardless of the grid resolution, we note that all but 12 of the cells are planar hexagons. Each of the hexagonal cells has $\boldsymbol{E}$ and $\boldsymbol{H}$ components distributed as shown in Fig. 3(a). Fig. 3(b) illustrates how the $\boldsymbol{E}$ and $\boldsymbol{H}$ components are distributed about each of the 12 planar pentagons.

Reference [21] describes in detail an optimization procedure for selecting the areas and locations of the hexagonal and pentagonal grid cells on the sphere to insure numerical consistency and to maximize the order of accuracy in the context of the Laplace operator. We have found that this optimization procedure also maximizes the observed accuracy of wave propagation about the sphere as governed by the 2-D TM Maxwell's equations.

III. FDTD ALGORITHM

A. Basic Algorithm

Ampere's Law in integral form [18] can be applied to develop an FDTD time-stepping relation for the electric field E_z at the center of the $(i, j)'$th grid cell. For example, referring to Fig. 3(a), for a hexagonal cell, we have

$$\begin{aligned}
E_z^{n+1}(i,j) = E_z^n(i,j) + \frac{\Delta t}{\varepsilon_0 S(i,j)} \\
\times \big\{ H_1^{n+0.5}(i-1, j-1)\Delta_{i,j}(1) \\
+ H_2^{n+0.5}(i-1, j-1)\Delta_{i,j}(2) \\
+ H_3^{n+0.5}(i-1, j-1)\Delta_{i,j}(3) \\
- H_1^{n+0.5}(i, j-1)\Delta_{i+1,j}(1) \\
- H_2^{n+0.5}(i, j)\Delta_{i+1,j+1}(2) \\
- H_3^{n+0.5}(i-1, j)\Delta_{i,j+1}(3) \big\}
\end{aligned} \quad (1)$$

where Δt is the time-step, $\Delta_{i,j}(n)$ is the nth wall length of the cell centered around $E_z(i,j)$ (where n is equal to 1, 2, or 3), and $S(i,j)$ is the area of the cell centered around $E_z(i,j)$.
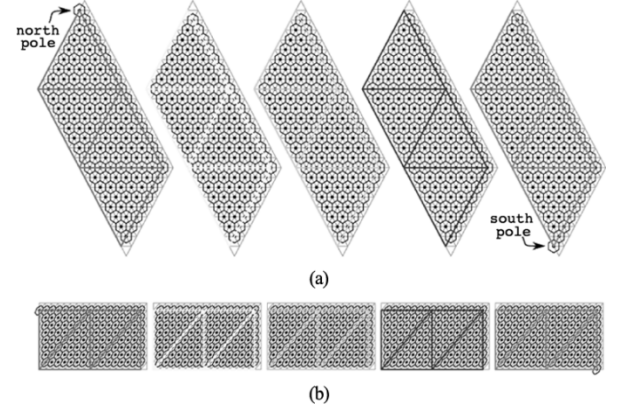

Fig. 2.   (a) Five ($im5 = 18, jm = 10$) grid panels of Fig. 1 after unwrapping and stretching them flat. The grid cells at the North and South Poles can be arbitrarily connected to any of the five panels. (b) Illustration of how the cells in the five grid panels of Fig. 1 can be assigned logically Cartesian coordinates, and how all five panels can then be laid side-by-side to constitute an overall ($im = 90$ and $jm = 10$) logically Cartesian grid [20].

TABLE I
HORIZONTAL ($im5$) AND VERTICAL (jm) NUMBER OF CELLS FOR THE FIVE PANELS AT DIFFERENT RESOLUTIONS

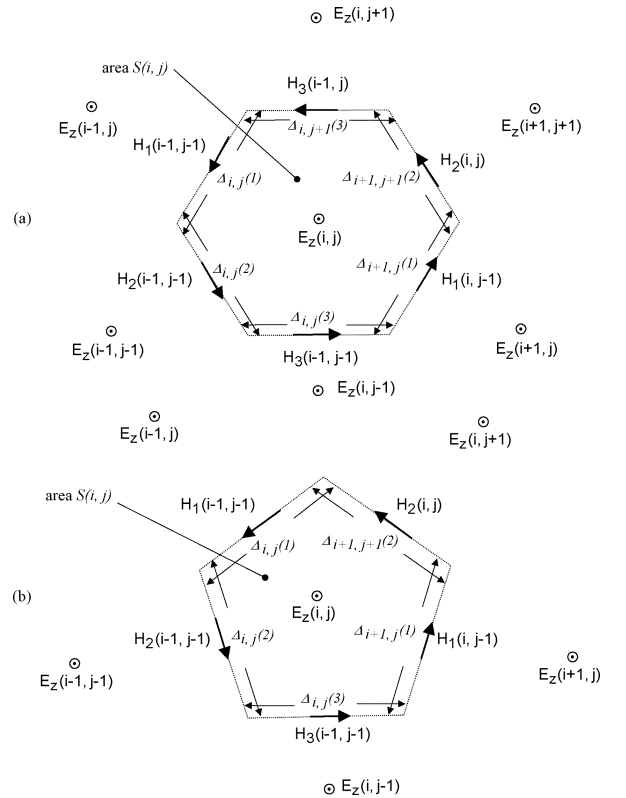| Number of cells	im5	jm
642	18	10
2,562	34	18
10,242	66	34
40,962	130	66
163,842	258	130
655,362	514	258

Fig. 3.   Details of the grid-cell geometry. (a) Hexagonal cell. (b) Pentagonal cell.

Similarly, referring to Fig. 3(b), the update for E_z at the center of a pentagonal cell at mid-latitude is given by

$$
\begin{aligned}
E_z^{n+1}(i,j) = E_z^n(i,j) + \frac{\Delta t}{\varepsilon_0 S(i,j)} \\
\times \big\{ H_1^{n+0.5}(i-1,j-1)\Delta_{i,j}(1) \\
+ H_2^{n+0.5}(i-1,j-1)\Delta_{i,j}(2) \\
+ H_3^{n+0.5}(i-1,j-1)\Delta_{i,j}(3) \\
- H_1^{n+0.5}(i,j-1)\Delta_{i+1,j}(1) \\
- H_2^{n+0.5}(i,j)\Delta_{i+1,j+1}(2) \big\}.
\end{aligned} \tag{2}
$$

In the same manner, the updates for E_z at the center of a pentagonal cell at the North and South Poles are given, respectively, by

$$
\begin{aligned}
E_z^{n+1}(1,jm-1) \\
= E_z^n(1,jm-1) + \frac{\Delta t}{\varepsilon_0 S(1,jm-1)} \\
\times \big\{ H_1^{n+0.5}(1,jm-2)\Delta_{2,jm-1}(1) \\
+ H_1^{n+0.5}(1,jm-2)\Delta_{2,jm-1}(1) \\
+ H_1^{n+0.5}(1,jm-2)\Delta_{2,jm-1}(1) \\
+ H_1^{n+0.5}(1,jm-2)\Delta_{2,jm-1}(1) \\
+ H_1^{n+0.5}(1,jm-2)\Delta_{2,jm-1}(1) \big\}
\end{aligned} \tag{3}
$$

$$
\begin{aligned}
E_z^{n+1}(im5-1,1) \\
= E_z^n(im5-1,1) + \frac{\Delta t}{\varepsilon_0 S(im5-1,1)} \\
\times \big\{ H_3^{n+0.5}(im5-2,1)\Delta_{im5-1,2}(3) \\
+ H_3^{n+0.5}(im5-2,1)\Delta_{im5-1,2}(3) \\
+ H_3^{n+0.5}(im5-2,1)\Delta_{im5-1,2}(3) \\
+ H_3^{n+0.5}(im5-2,1)\Delta_{im5-1,2}(3) \\
+ H_3^{n+0.5}(im5-2,1)\Delta_{im5-1,2}(3) \big\}
\end{aligned} \tag{4}
$$

where the $\Delta_{i,j}(n)$ and the H_1 or H_3 component having the indicated coordinates from each of the five panels are used.

The FDTD time-stepping algorithm is completed by specifying the updates for the H-fields using Faraday's Law in integral form [18]. For example, referring to the grid cells shown in Figs. 3(a) and 3(b), we have, for $\delta_n(i,j)$ the distance between adjacent E_z's at $H_n(i,j)$, (5)–(7), as shown at the bottom of the page.

B. Grid Wrap-Around (Periodic Boundary Condition)

For each of the five panels, only the $E_z(i,j)$ components for which $2 \leq i \leq (im5-1)$ and $2 \leq j \leq (jm-1)$, along with the E_z components for the two pentagons at the North and South Poles are updated according to the algorithm presented in

above. The ghost E_z field components, i.e. for $(i=1, 1 \leq j \leq jm-2)$, $(j=1, 1 \leq i \leq im5-2)$, $(i=im5, 2 \leq j \leq jm-1)$, and $(j=jm, 2 \leq i \leq im5)$, along with $(i=1, j=jm-1)$ and $(i=im5-1, j=1)$ for the four panels not updating the North and South Poles, are then filled after each time step by setting them equal to the corresponding E_z component in the neighboring panel.

IV. RESULTS

We now report the results of numerical experiments designed to test the efficiency and accuracy of our new geodesic FDTD grid model for 2-D TM electromagnetic wave propagation about the lossless Earth-sphere. The idea here is to track an impulsive circular cylindrical wave in time and space as it propagates radially outward from a filamentary current source, travels completely around the Earth-sphere model, and then propagates radially inward to the antipode. Results are shown for a geodesic FDTD grid with 40 962 cells ($im5 = 130$ and $jm = 66$) spanning the Earth-sphere, with the time step $\Delta t = 25\ \mu s$. For this simulation, implemented in Fortran 90 on a Dell 530 workstation running Linux, the required computer memory is 3.3 MB and the running time 2.5 min for a single wave circumnavigation of the Earth-sphere. In comparison, a comparably resolved latitude-longitude FDTD grid of the type introduced in [11] and [12] would require 2.4 MB and 34 min running time on the same computer. We see that the geodesic FDTD grid executes about 14-times faster while requiring only about 1.4-times more data storage in two dimensions.

Fig. 4 is a snapshot visualization of the electric field calculated using the new geodesic FDTD grid model projected onto the surface of the Earth-sphere as the radiated wave converges to the antipode. Superimposed on this visualization is: 1) a sample computed contour of equal-amplitude electric field; and 2) a circle centered at the antipode that is drawn to have a radius matching as well as possible that of the equal-amplitude electric field contour. We see that there is negligible deviation of the computed equal-amplitude electric field contour from the circle. This means that the impulsive numerical wave has propagated from its source point almost completely to the antipode in an azimuthally isotropic manner despite passing through regions of hexagonal and pentagonal grid cells of varying areas. By way of comparison, using this same test, the azimuthal isotropy of wave propagation within the latitude-longitude FDTD grid introduced in [11] and [12] is poorer by approximately one order-of-magnitude for grids of comparable spatial resolution.

Fig. 5 graphs the calculated time-waveform of the electric field at the antipode for the first two circumnavigations of the Earth-sphere. This figure shows the 180° phase reversals of the

$$
H_1^{n+1.5}(i-1,j-1) = H_1^{n+0.5}(i-1,j-1) + \frac{\Delta t}{\mu_0 \delta_1(i-1,j-1)}\left[E_z^{n+1}(i-1,j) - E_z^{n+1}(i,j)\right] \tag{5}
$$

$$
H_2^{n+1.5}(i-1,j-1) = H_2^{n+0.5}(i-1,j-1) + \frac{\Delta t}{\mu_0 \delta_2(i-1,j-1)}\left[E_z^{n+1}(i-1,j-1) - E_z^{n+1}(i,j)\right] \tag{6}
$$

$$
H_3^{n+1.5}(i-1,j-1) = H_3^{n+0.5}(i-1,j-1) + \frac{\Delta t}{\mu_0 \delta_3(i-1,j-1)}\left[E_z^{n+1}(i,j-1) - E_z^{n+1}(i,j)\right]. \tag{7}
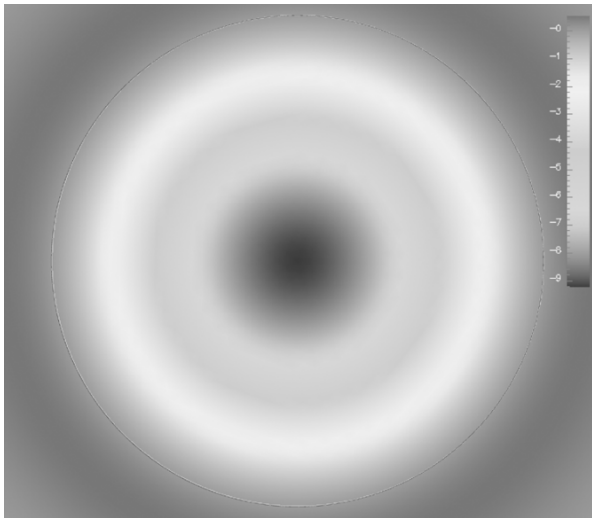$$

Fig. 4.   Visualization of the electric field projected onto the surface of the Earth-sphere as the radiated wave converges to the antipode. Note that the white contour of calculated equal-amplitude electric field coincides almost exactly with a black dotted circle centered on the antipode.
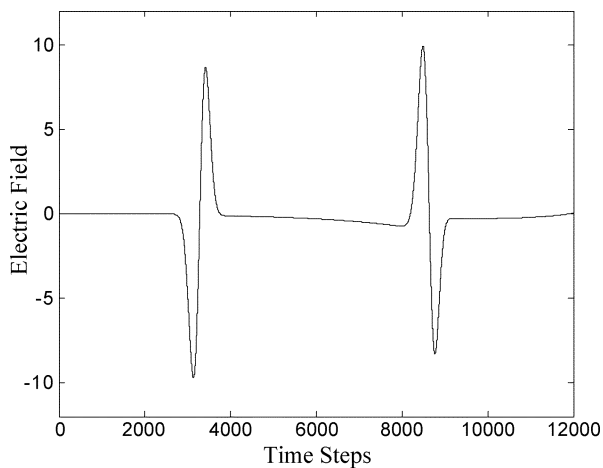

Fig. 5.   Calculated time-waveform of the electric field at the antipode for the first two circumnavigations of the Earth-sphere.

electric-field at the antipode first calculated by Wait [4]. Further, this figure shows a 0.134-s circumnavigation period, corresponding to a 7.46-Hz fundamental resonance of the lossless 2-D Earth model. This is virtually the same as that obtained previously by a comparably resolved latitude–longitude FDTD grid [11], [12].

V. CONCLUSION AND ONGOING WORK

We have presented a new geodesic FDTD grid model for 2-D TM electromagnetic wave propagation about the Earth-sphere that is considerably superior to our previously reported latitude-longitude grid. The new grid model is simpler to construct, avoids geometrical singularities at the poles, executes about 14-times faster, and provides much more isotropic wave propagation. It will also permit an easier interchange of data with state-of-the-art Earth-simulation codes widely used by the geophysics community.

We are currently extending the 2-D TM FDTD spherical geodesic grid discussed here to a fully 3-D space lattice filling the complete Earth-ionosphere volume. This will permit accounting of vertical as well as horizontal inhomogeneities of the excitation, atmosphere, and Earth. We plan to couple this model to emerging whole-Earth geophysical codes now under development for the study of seismic phenomena, including earthquake precursors [22].

REFERENCES

[1]   J. R. Wait, "Terrestrial propagation of very-low-frequency radio waves: a theoretical investigation," *J. Res. Nat. Bureau Stand.*, vol. 64D, p. 153, 1960.
[2]   K. G. Budden, "The influence of the Earth's magnetic field on radio propagation by waveguide modes," *Proc. Royal Soc. A*, vol. 265, p. 538, 1962.
[3]   J. R. Wait, "Earth-ionosphere cavity resonances and the propagation of ELF radio waves," *Radio Sci.*, vol. 69D, p. 1057, 1965.
[4]   ——, "Distortion of ELF pulses after propagation through an antipode," *J. Geophys. Res.*, vol. 74, pp. 2982–2986, 1969.
[5]   ——, *Electromagnetic Waves in Stratified Media*.   New York: Pergamon, 1970.
[6]   ——, "Reflection of VLF radio waves at a junction in the earth-ionosphere waveguide," *IEEE Trans. Electromagn. Compat.*, vol. 34, pp. 4–8, Feb. 1992.
[7]   S. A. Cummer, U. S. Inan, T. F. Bell, and C. P. Barrington-Leigh, "ELF radiation produced by electrical currents in sprites," *Geophys. Res. Lett.*, vol. 25, p. 1281, 1998.
[8]   E. R. Williams, "The Schumann resonance—a global tropical thermometer," *Science*, vol. 256, p. 1184, 1992.
[9]   D. W. Strangway, C. M. Swift, and R. C. Holmer, "The application of audio-frequency magnetotellurics to mineral exploration," *Geophys.*, vol. 38, p. 1159, 1975.
[10] M. Parrot, "Statistical study of ELF/VLF emissions recorded by a low-altitude satellite during seismic events," *J. Geophys. Res.*, vol. 99, p. 23 339, 1994.
[11] J. Simpson and A. Taflove, "Two-dimensional FDTD modeling of impulsive ELF antipodal propagation about the Earth-sphere," in *Proc. IEEE AP-S Int. Symp.*, vol. 3, San Antonio, TX, June 2002, pp. 678–681.
[12] ——, "Two-dimensional FDTD model of antipodal ELF propagation and Schumann resonance of the Earth," *IEEE Antennas Wireless Propagat. Lett.*, vol. 1, pp. 53–56, Dec. 2002.
[13] ——, "Global three-dimensional FDTD modeling of impulsive ELF propagation about the Earth," in *Proc. IEEE AP-S Int. Symp.*, Columbus, OH, June 2003, pp. 940–944.
[14] J. J. Simpson and A. Taflove, "Three-dimensional FDTD modeling of impulsive ELF propagation about the Earth-sphere," *IEEE Trans. Antennas Propagat.*, vol. 52, pp. 443–451, Feb. 2004.
[15] *http://www.ece.northwestern.edu/ecefaculty/taflove/3Dmovietext@gif.avi* [Online]
[16] M. Hayakawa and T. Otsuyama, "FDTD analysis of ELF wave propagation in inhomogeneous subionospheric waveguide models," *ACES J.*, vol. 17, no. 3, pp. 239–244, Nov. 2002.
[17] T. Otsuyama, D. Sakuma, and M. Hayakawa, "FDTD analysis of ELF wave propagation and Schumann resonances for a subionospheric waveguide model," *Radio Sci.*, 2004, to be published.
[18] A. Taflove and S. C. Hagness, *Computational Electrodynamics: The Finite-Difference Time-Domain Method*, 2nd ed.   Norwood, MA: Artech House, 2000.
[19] R. Holland, "THREDS: a finite-difference time-domain EMP code in 3D spherical coordinates," *IEEE Trans. Nucl. Sci.*, vol. NS-30, pp. 4592–4595, Dec. 1983.
[20] D. A. Randall, T. D. Ringler, and R. P. Heikes, "Climate modeling with spherical geodesic grids," *Comput. Sci. Eng.*, vol. 4, no. 5, pp. 32–41, Sept./Oct. 2002.
[21] R. P. Heikes and D. A. Randall, "Numerical integration of the shallow-water equations on a twisted icosahedral grid. Part II: a detailed description of the grid and an analysis of numerical accuracy," *Month. Weather Rev.*, vol. 123, pp. 1881–1887, June 1995.
[22] APEC cooperation for earthquake simulation (ACES) *http://shake2. earthsciences.uq.edu.au/ACES/* [Online]